Three-Dimensional Imaging of Lipid Gene-Carriers: Membrane Charge Density Controls Universal Transfection Behavior in Lamellar Cationic Liposome-DNA Complexes

Alison J. Lin,* Nelle L. Slack,* Ayesha Ahmad,* Cyril X. George,† Charles E. Samuel,† and Cyrus R. Safinya*

*Materials Department, Physics Department, and Biomolecular Science and Engineering Program, University of California, Santa Barbara, California 93106; and †Molecular, Cellular, and Developmental Biology Department, and Biomolecular Science and Engineering Program, University of California, Santa Barbara, California 93106

ABSTRACT Cationic liposomes (CLs) are used worldwide as gene vectors (carriers) in nonviral clinical applications of gene delivery, albeit with unacceptably low transfection efficiencies (TE). We present three-dimensional laser scanning confocal microscopy studies revealing distinct interactions between CL-DNA complexes, for both lamellar L_α^C and inverted hexagonal H_{II}^C nanostructures, and mouse fibroblast cells. Confocal images of L_α^C complexes in cells identified two regimes. For low membrane charge density (σ_M), DNA remained trapped in CL-vectors. By contrast, for high σ_M, released DNA was observed in the cytoplasm, indicative of escape from endosomes through fusion. Remarkably, firefly luciferase reporter gene studies in the highly complex L_α^C-mammalian cell system revealed an unexpected simplicity where, at a constant cationic to anionic charge ratio, TE data for univalent and multivalent cationic lipids merged into a single curve as a function of σ_M, identifying it as a key universal parameter. The universal curve for transfection by L_α^C complexes climbs exponentially over $\approx$ four decades with increasing σ_M below an optimal charge density (σ_M^*), and saturates for $\sigma_M > \sigma_M^*$ at a value rivaling the high transfection efficiency of H_{II}^C complexes. In contrast, the transfection efficiency of H_{II}^C complexes is independent of σ_M. The exponential dependence of TE on σ_M for L_α^C complexes, suggests the existence of a kinetic barrier against endosomal fusion, where an increase in σ_M lowers the barrier. In the saturated TE regime, for both L_α^C complexes and H_{II}^C, confocal microscopy reveals the dissociation of lipid and DNA. However, the lipid-released DNA is observed to be in a condensed state, most likely with oppositely charged macro-ion condensing agents from the cytoplasm, which remain to be identified. Much of the observed bulk of condensed DNA may be transcriptionally inactive and may determine the current limiting factor to transfection by cationic lipid gene vectors.

INTRODUCTION

The unrelenting research activity involving gene therapy with either synthetic vectors (carriers) or engineered viruses is currently unprecedented (Alper, 2002; Chesnoy and Huang, 2000; Clark and Hersh, 1999; Ferber, 2001; Henry, 2001; Mahato and Kim, 2002; Miller, 1998). After the initial landmark studies (Felgner et al., 1987; Nabel et al., 1993; Singhal and Huang, 1994), cationic liposomes (CLs; closed bilayer membrane shells of lipid molecules) have emerged worldwide as the most prevalent synthetic vectors (carriers) (Ferber, 2001) whose mechanisms of action are investigated extensively in research laboratories, concurrently with ongoing, mostly empirical, clinical trials to develop cancer vaccines (Alper, 2002; Chesnoy and Huang, 2000; Clark and Hersh, 1999; Ferber, 2001; Henry, 2001; Mahato and Kim, 2002; Miller, 1998). Primary among the advantages of CL over viral methods is the lack of immune response due to the absence of viral peptides and proteins. Moreover, while viral capsids have a maximum DNA-carrying capacity of ~40 kbp, CLs (which, when combined with DNA, form, in most instances, self-assemblies with distinct lamellar L_α^C or inverted hexagonal H_{II}^C nanostructures; see Raedler et al., 1997; Koltover et al., 1998; Lasic et al., 1997), place no limit on the size of the DNA. Thus, if complexed, for example, with human artificial chromosomes (Wilard, 2000), optimally designed CL-carriers offer the potential of potent vectors comprised of multiple human genes and regulatory sequences extending over hundreds of thousands of DNA base pairs.

Despite all the promise of CLs as gene vectors, their transfection efficiency (TE; ability to transfer DNA into cells followed by expression), compared to viral vectors, remains notoriously low, resulting in a flurry of research activity aimed at enhancing transfection (Alper, 2002; Chesnoy and Huang, 2000; Clark and Hersh, 1999; Ferber, 2001; Henry, 2001; Mahato and Kim, 2002; Miller, 1998). A further sense of urgency for developing efficient synthetic carriers stems from the recent tragic events associated with the use of engineered adenovirus vectors leading to the death of a patient due to an unanticipated severe immune response (Marshall, 2000). In addition, in the latest gene therapy trials using modified retrovirus vectors to treat children with severe combined immunodeficiency, a French gene therapy team has reported a major setback where one patient (out of eleven) developed a blood disorder similar to leukemia which is confirmed to have resulted from insertion of the modified retrovirus in the initial coding region of a gene related to the

Submitted October 3, 2002, and accepted for publication December 18, 2002.

Alison J. Lin and Nelle L. Slack contributed equally to this work.

Address reprint requests to C. R. Safinya, MRL Rm. 2208, University of California, Santa Barbara, CA 93106. Tel.: 805-893-8635; Fax: 805-893-7221; E-mail: safinya@mrl.ucsb.edu.

Our in vitro studies should apply to TE optimization in ex vivo cell transfection, where cells are removed and returned to patients after transfection. In particular, our studies, aimed at understanding the chemically and physically dependent mechanisms underlying TE in continuous (dividing) cell lines, should aid clinical efforts to develop efficient CL-vector cancer vaccines in ex vivo applications. The vaccines are intended to induce transient expression of genes coding for immunostimulatory proteins in dividing cells (Chesnoy and Huang, 2000; Nabel et al., 1993; Rinehart et al., 1997; Stopeck et al., 1998); thus, the nuclear membrane, which dissolves during mitosis, is not considered a barrier to expression of DNA.

A critical requirement for enhancing transfection via synthetic carriers is a full understanding of the different nanostructures of CL-DNA complexes and the physical and chemical basis of interactions between complexes and cellular components. Toward that end, we used a combination of three-dimensional laser scanning confocal microscopy (LSCM), which closely followed complexes across the plasma membrane and inside the cytoplasm, and reporter gene TE studies that gave a statistically meaningful measure of the total amount of protein synthesized by cells from delivered DNA. Furthermore, we examined the structure-dependent basis of transfection through imaging of CL-DNA complexes exhibiting either the L_α^C (cationic lipid DOTAP mixed with neutral lipid DOPC) or H_{II}^C (DOTAP mixed with neutral lipid DOPE) nanostructure (Koltover et al., 1998; Raedler et al., 1997). Previous to our report, TE studies had shown that in mixtures of DOTAP and neutral lipids, typically at a wt.:wt. ratio of between 1:1 and 1:3, DOPE aided, while DOPC severely suppressed, transfection (Farhood et al., 1995; Hui et al., 1996), hence suggesting that H_{II}^C complexes transfect more efficiently than L_α^C complexes.

MATERIALS AND METHODS

Materials

Lipids included univalent cationic lipids DOTAP (1,2-dioleoyl-3-trimethylammonium-propane) and DMRIE (*n*-(2-hydroxyethyl)-*n*,*n*-dimethyl-2,3-bis(tetradecyloxy)-1-propanaminium), multivalent cationic lipid DOSPA (2,3-Dioleyloxy-*n*-(2-(sperminecarboxamido)ethyl)-*n*,*n*-dimethyl-1-propaniminium penta-hydrochloride), and neutral lipids DOPC (1,2-dioleoyl-*sn*-glycero-3-phosphocholine) and DOPE (1,2-dioleoyl-*sn*-glycero-3-phosphoethanolamine). DOTAP, DOPC, DOPE were purchased from Avanti Polar Lipids, Inc., and DMRIE and DOSPA were gifts from Vical Inc. Plasmid DNA containing the Luciferase gene and SV40 promoter/enhancer elements was used (pGL3-control vector, Promega, Cat. E1741).

Cell culture

Mouse fibroblast L-cell lines were subcultured in DMEM (Dulbecco's modified Eagle's medium, Gibco BRL) supplemented with 1% (vol/vol) penicillin-streptomycin (Gibco BRL) and 5% (vol/vol) fetal bovine serum (HyClone Lab) at 37°C and 5% CO_2 atmosphere every 2–4 days to maintain monolayer coverage.

Liposome preparation

Neutral lipids (DOPE, DOPC) were dissolved in chloroform and cationic lipids (DOTAP, DOSPA, DMRIE) were dissolved in a chloroform/methanol mixture. The lipid solutions were mixed in required ratios and the solvent was evaporated, first under a stream of nitrogen and then in vacuum over night, leaving a lipid film behind. The appropriate amount of millipore water was added to the dried lipid film, resulting in the desired concentration (0.1 mg/ml–25 mg/ml) and incubated at 37°C for at least 6 h to allow formation of liposomes. To form small unilamellar vesicles, liposome solutions were vortexed for 1 min, tip-sonicated to clarity (for 5–10 min), and filtered with 0.2 μm filters to remove metal particulates arising from the sonicator tip. Liposome solutions were then stored at 4°C.

Transfection

L-cells were transfected at a confluency of 60–80%. Using liposome (0.5 mg/ml) and DNA (1 mg/ml) stock solutions, CL-DNA complexes were prepared in DMEM, which contained 2 μg of pGL3-DNA at a cationic-to-anionic charge ratio of 2.8 and allowed to sit for 20 min for complex formation. The cells were then incubated with complexes for 6 h, the optimized time of transfer into cells before removal, rinsed three times with phosphate-buffered saline (Gibco BRL), and incubated in supplemented DMEM for an additional 24 h (sufficient for a complete cell cycle) to allow expression of the luciferase gene. Luciferase gene expression was measured with the Luciferase Assay System from Promega. Each transfection experiment was repeated between 3–6 times over a short period of a few days yielding the error bars (Slack, 2000; Lin et al., 2002). In addition, the experiments were repeated four times over a 12-month period using different cell batches. While the absolute value of the average of each transfection measurement between the different experiments (done with several months separating experiments) varied by as much as a decade (which is also commonly found by other groups; Boussif et al., 1995), the observed trend in the transfection data was completely reproducible. Transfection efficiency was normalized to mg of total cellular protein using the Bio-Rad Protein Assay Dye Reagent Concentration solution (Bio-Rad) and is expressed as relative light units per mg of total cellular protein $\pm$ 1 SD. The transfection protocol is commonly used by others (Boussif et al., 1995).

Laser scanning confocal microscopy (LSCM)

L-cells were seeded on coverslips in six-well plates and allowed to grow, reaching a confluency of 60–80%. DNA was labeled following the Mirus Label IT (PanVera Corporation) protocol, which is fluorescent at 492 nm. Lipids were labeled with 0.2% (wt) Texas Red DHPE (Molecular Probes), which is fluorescent at 583 nm. Using labeled liposome (0.5 mg/ml) and DNA (0.1 mg/ml) stock solutions, CL-DNA complexes were prepared in DMEM using 2 μg of pGL3-DNA (at a cationic to anionic charge ratio of 2.8), allowed to sit for 20 min for complex formation, and incubated with cells for the optimal 6-h transfer time. Cells were rinsed three times with phosphate-buffered saline (Gibco BRL), fixed by soaking in a fixing solution (3.7% formaldehyde in PBS) for 20–30 min and mounted using SlowFade Light Antifade Kit (Molecular Probes) for microscopy. Confocal images were taken with a Leica DM IRBE confocal microscope. The images of Figs. 3 and 5 (repeated more than 10 times) are representative of the typical behavior in a given field of view (Lin, 2001).

X-ray diffraction (XRD)

The XRD experiments were carried out at the Stanford Synchrotron Radiation Laboratory at 10 KeV. To prepare CL-DNA samples liposome solutions (25 mg/ml) and DNA solutions (5 mg/ml) were each diluted in DMEM at 1:1 (vol.:vol.), then mixed at the desired cationic to anionic charge ratio of 2.8 and centrifuged before loading into for 1.5-mm x-ray. We

note that similar to previous findings (Koltover et al., 1998; Raedler et al., 1997) the self-assembled structures of CL-DNA complexes does not change in the concentration range between the x-ray samples and the samples for confocal microscopy and transfection.

RESULTS AND DISCUSSION

The initial electrostatic attraction between positively charged CL-DNA complexes and mammalian cells is known to be mediated by negatively charged cell surface sulfated proteoglycans (Fig. 1 *a*, *expanded view*; also see Mislick and Baldeschwieler, 1996). Consistent with previous studies, we found that L_α^C complexes gain entry into the cell through endocytosis (Fig. 1, *b* and *c*; see also Labat-Moleur et al., 1996; Zabner et al., 1995). LSCM of L_α^C CL-DNA particles in cells revealed two distinct types of behavior. At low membrane charge density, $\sigma_M \approx 0.005\ e/\text{Å}^2 = e/(200\ \text{Å}^2)$, mostly intact L_α^C complexes were present inside cells implying that DNA was trapped by the lipid vector. Further TE experiments confirmed that the intact complexes were themselves trapped in endosomes (Fig. 1 *c*). At high $\sigma_M \approx 0.012\ e/\text{Å}^2 \approx e/(83\ \text{Å}^2)$, we observed released DNA inside cells consistent with the escape of CL-DNA complexes into the cytoplasm through fusion with anionic endosomal membranes (Fig. 1 *d*). LSCM further determined that the released DNA was condensed (Fig. 1 *e*), most likely, with oppositely charged cytoplasmic condensing agents absent in endosomes. Unlike the endosomal environment, the cytoplasm contains many multivalent cationic biomolecules such as spermine and histones, which become available during the cell cycle in millimolar concentration levels, and are able to condense DNA (Bloomfield, 1991).

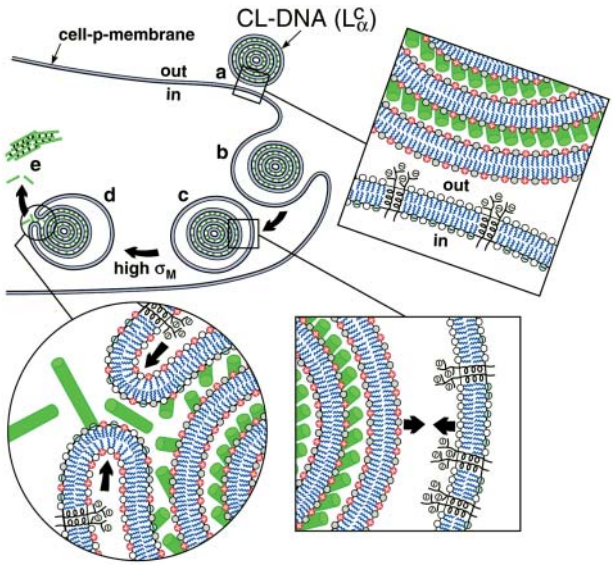

FIGURE 1 Model of cellular uptake of L_α^C complexes. (*a*) Cationic complexes adhere to cells due to electrostatic attraction between positively charged CL-DNA complexes and negatively charged cell-surface sulfated proteoglycans (shown in expanded views) of mammalian plasma membranes. (*b* and *c*) After attachment, complexes enter through endocytosis. (*d*) Only those complexes with a large enough membrane charge density (σ_M) escape the endosome through activated fusion with endosomal membranes. (*e*) Released DNA inside the cell is observed by comfocal microscopy to be present primarily in the form of aggregates. The DNA aggregates must reside in the cytoplasm because oppositely charged cellular biomolecules able to condense DNA are not present in the endosome. Arrows in the expanded view of *c* indicate the electrostatic attraction between the positively charged membranes of the complex and the negatively charged membranes of the endosome (comprised of sulfated proteoglycans and anionic lipids), which tends to enhance adhesion and fusion. Arrows in the expanded view in *d* indicate that the bending of the membranes hinders fusion.

Corresponding TE measurements exhibited two remarkable features. First and foremost, an unexpected simplicity emerged from this highly complex L_α^C-cell system, where σ_M was found to be a universal parameter controlling TE. The TE data for L_α^C complexes containing DOPC mixed with the multivalent cationic lipid DOSPA or the univalent cationic lipids DOTAP and DMRIE, at a constant cationic to anionic charge ratio, merged onto a universal curve when plotted versus σ_M. Second, this universal TE curve increased exponentially, over four decades, with increasing σ_M. This behavior is consistent with a model describing a kinetic barrier for fusion of CL-DNA complexes with the endosomal membrane (Fig. 1 *d*), where an increase in σ_M lowers the barrier height. This new understanding of the fundamental role of the lipid carrier σ_M has led to redesigned L_α^C DOPC-based carriers with efficacy competitive with the TE of H_{II}^C DOPE-based carriers.

We used positively charged CL-DNA complexes prepared at ρ = DOTAP/DNA (wt./wt.) = 6 ($\rho = 2.2$ is the isoelectric point) from mixtures of cationic and neutral lipids complexed with plasmid DNA (pGL3). The weight ratio $\rho = 6$, which gave a cationic-to-anionic charge ratio of 2.8, was chosen as it corresponded to the middle of a typical plateau region observed for optimal transfection conditions as a function of increasing ρ above the isoelectric point. X-ray diffraction (XRD) results elucidated the structures of these complexes in water and in DMEM, a common environment for in vitro studies of cells. Synchrotron XRD of DOTAP/DOPC complexes at the mole fraction $\Phi_{DOPC} = 0.67$ (Fig. 2, *left*) showed sharp peaks at $q_{001} = 0.083\ \text{Å}^{-1}$, $q_{002} = 0.166\ \text{Å}^{-1}$, with a shoulder peak at $q_{003} = 0.243\ \text{Å}^{-1}$ (due to the form factor), and $q_{004} = 0.335\ \text{Å}^{-1}$, resulting from the layered structure of the L_α^C phase (d = interlayer spacing = $\delta_m + \delta_w = 2\pi/q_{001} = 75.70$ Å) with DNA intercalated between cationic lipid bilayers (Fig. 2, *left*, *inset*). For DOTAP/DOPE complexes at $\Phi_{DOPE} = 0.69$, XRD (Fig. 2, *right*) revealed four orders of Bragg peaks at $q_{10} = 0.103\ \text{Å}^{-1}$, $q_{11} = 0.178\ \text{Å}^{-1}$, $q_{20} = 0.205\ \text{Å}^{-1}$, and $q_{21} = 0.270\ \text{Å}^{-1}$, denoting the H_{II}^C phase (Fig. 2, *right*, *inset*) with a unit cell spacing of $a = 4\pi/(\sqrt{3}q_{10}) = 70.44$ Å. Except for a difference in lattice constants, the structures of CL-supercoiled DNA complexes are analogous to the ones reported recently for CL-linear DNA complexes (Koltover et al., 1998, 1999; Raedler et al., 1997; Salditt et al., 1997).

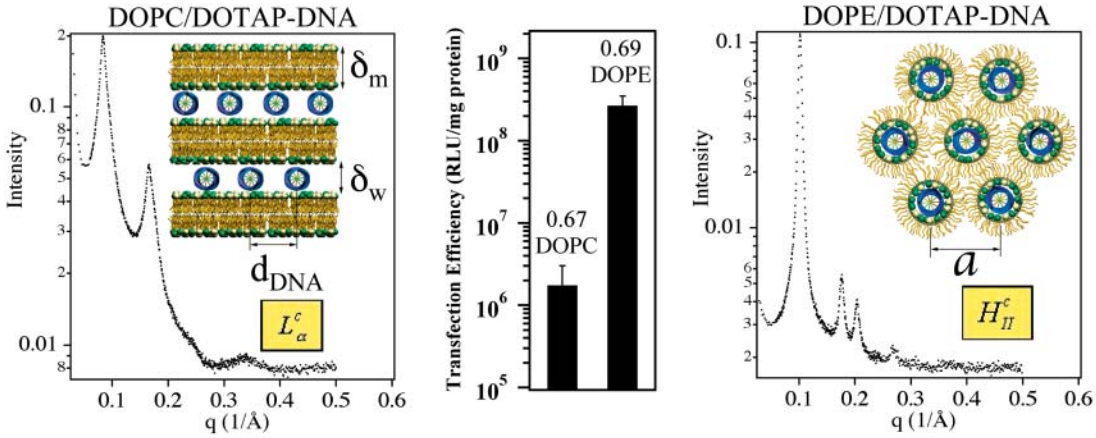

FIGURE 2 Comparison of structure and transfection efficiency (TE). Left (mole fraction $\Phi_{DOPC} = 0.67$) shows a typical XRD scan of lamellar (*inset*) L_α^C complexes. Right (mole fraction $\Phi_{DOPE} = 0.69$) shows a typical XRD scan of inverted hexagonal (*inset*) H_{II}^C complexes. Middle displays the corresponding TE, as measured by luciferase enzyme assays of transfected mouse L-cells.

Transfection experiments were done using plasmid DNA (pGL3), which contains the firefly luciferase reporter gene, to measure TE and its correlation to the solution structures of complexes. Mouse L-cells were transfected with CL-DNA complexes and incubated on average for at least a full cell-cycle, during which expression occurred. A standard luciferase assay allowed us to evaluate quantitatively the amount of synthesized protein by measuring the bioluminescence (number of emitted photons) in relative light units per mg of cell protein. Fig. 2 (*middle*) clearly demonstrates the higher TE, by more than two decades, attained by complexes in the H_{II}^C phase at $\Phi_{DOPE} = 0.69$ compared to L_α^C complexes at $\Phi_{DOPC} = 0.67$.

To further understand the structure-function correlation, we examined the transfer process of CL-DNA complexes into cells and the mechanism of the subsequent DNA release using LSCM, which provides an optical resolution of ~0.3 μm in the x and y, and ~3/4 μm in the z. The complexes were doubly tagged with fluorescent labels, a red one for lipid and a green covalent one for DNA. Fig. 3 shows LSCM pictures of mouse L-cells after 6 h of transfer time. By comparing images of the x-y, y-z, and x-z planes, we were able to determine the position of an object relative to a cell. Fig. 3 *A* shows a typical confocal image of a mouse cell transfected with H_{II}^C complexes at $\Phi_{DOPE} = 0.69$. The lipid fluorescence clearly outlines the plasma membrane, indicating fusion of lipid with the plasma membrane before or after entry through the endocytic pathway (Wrobel and Collins, 1995). An aggregate of complexes (*yellow*) was seen inside a cell as well as a clump of DNA (*green*) in the cytoplasm. The image shows that the interaction between H_{II}^C complexes and cells leads to the dissociation and release of DNA from the CL-vector consistent with the measured high TE.

The corresponding confocal images with L_α^C complexes at $\Phi_{DOPC} = 0.67$ are shown in Fig. 3 *B*. In striking contrast to transfection with H_{II}^C complexes, we observed no free DNA, but rather many individual intact CL-DNA complexes inside cells. Fig. 3 *B* highlights one such typical complex. In the absence of fusion, complexes entered cells through endocytosis (Fig. 1). This was further substantiated in LSCM images of cells prepared at 4°C, where endocytosis is inhibited, which showed complexes attached to the outside cell surface and none within the cell body (Lin et al., 2000; Lin, 2001; Safinya et al., 2002). At $\Phi_{DOPC} = 0.67$, most of the DNA remained trapped by the CL-vector consistent with the measured low TE. As we discuss below, chloroquine-based experiments showed that the intact CL-DNA complexes were typically trapped within endosomes.

As the concentration of DOPC decreased in the L_α^C CL-DNA complexes, we observed an unexpected enhancement in TE by two decades. Fig. 4 *A* (*red diamonds*) exhibits the nontrivial dependence of TE on Φ_{DOPC} for DOPC/DOTAP-DNA complexes, which starts low for $0.5 < \Phi_{DOPC} < 0.7$ and increases dramatically to a value, at $\Phi_{DOPC} = 0.2$, rivaling that achieved by DOPE/DOTAP-DNA complexes. Similar results were obtained for another univalent cationic lipid DMRIE (Fig. 4 *A*, *black triangles*). The key experiment, which led to a deeper understanding of TE, was a study done with the multivalent cationic lipid DOSPA (*blue squares*) replacing DOTAP. A qualitatively similar trend was observed with TE decreasing rapidly above a critical Φ^*_{DOPC}, albeit with Φ^*_{DOPC} shifted from ~0.2 (observed for DOTAP and DMRIE complexes) to 0.7 ± 0.1 (DOSPA). The main difference between the cationic lipids is the notably larger charge density of DOSPA (Fig. 4 *B*, *inset*), with a larger headgroup carrying potentially up to five cationic charges. Thus, at a given Φ_{DOPC}, the membrane charge density (σ_M) is significantly larger in DOSPA compared to DOTAP or DMRIE containing complexes.

We show in Fig. 4 *B* the same TE data of Fig. 4 *A*, now plotted versus the membrane charge density σ_M (i.e., the average charge per unit area of the cationic membrane):

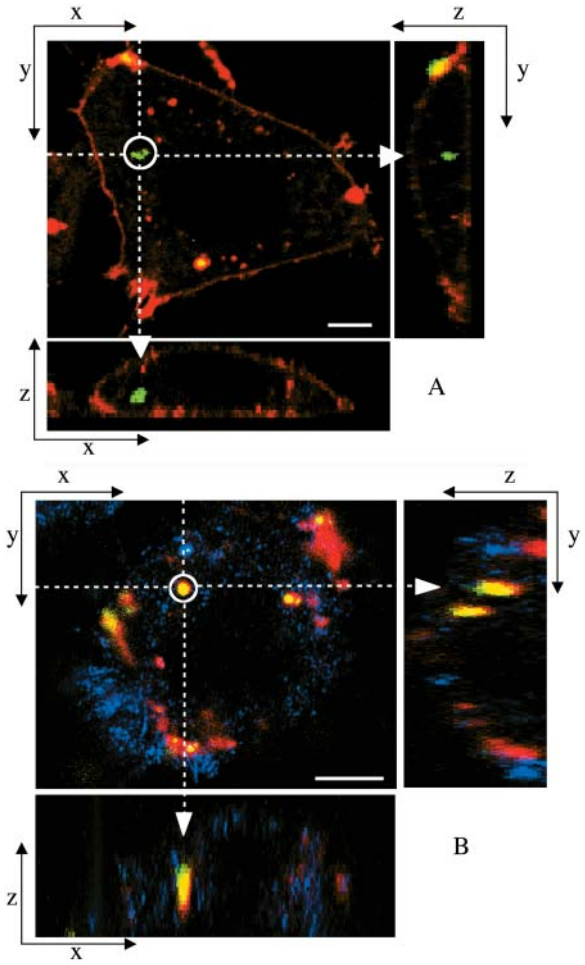

FIGURE 3 Laser scanning confocal microscopy (LSCM) images of transfected mouse L-cells. Red denotes lipid; green, DNA; and yellow, the overlap of the two denotes CL-DNA complexes. For each set, middle is the *x*-*y* top view at a given *z*; right is the *y*-*z* side view along the vertical dotted line; bottom is the *x*-*z* side view along the horizontal dotted line. Objects in circles are indicated by arrows in the *x*-*z* and *y*-*z* plane side views. (*A*) Cells transfected with H_{II}^{C} complexes ($\Phi_{DOPE} = 0.69$), show fusion of lipid (*red*) with the cell plasma membrane and the release of DNA (*green in the circle*) within the cell. Thus, H_{II}^{C} complexes display clear evidence of separation of lipid and DNA, which is consistent with the high transfection efficiency of such complexes. The released exogenous DNA is in an aggregated state, which implies that it has been condensed with oppositely charged biomolecules of the cell, which remain to be identified. (*B*) Cells transfected with L_{α}^{C} complexes at $\Phi_{DOPC} = 0.67$, which results in a low membrane charge density $\sigma_M \approx 0.005\ e/\text{Å}^2$ and low transfection efficiency (as plotted in Fig. 4 *B*). First, no fusion is observed. Second, intact CL-DNA complexes are observed inside cells (one such yellow complex is shown in the circle). The intact complex implies that DNA remains trapped within the complex, which is consistent with the observed low transfection efficiency of such low σ_M/L_{α}^{C} complexes. Because of the lack of fusion (which aided observation of the cell outline in *A*), we achieved cell outline by observation in reflection mode, which appears as blue. Bars = 5 μm applies to all planes.

$$\sigma_M = eZN_{cl}/(N_{nl}A_{nl}+N_{cl}A_{cl}) = [1-\Phi_{nl}/(\Phi_{nl}+r\Phi_{cl})]\sigma_{cl}. \quad (1)$$

Here, N_{nl} and N_{cl} are the number of neutral and cationic lipids, respectively; $r = A_{cl}/A_{nl}$ is the ratio of the headgroup area of the cationic to neutral lipid; $\sigma_{cl} = eZ/A_{cl}$ is the charge density of the cationic lipid with valence Z; and $\Phi_{nl} = N_{nl}/(N_{nl} + N_{cl})$ and $\Phi_{cl} = N_{cl}/(N_{nl} + N_{cl})$ are the mole fractions of the neutral and cationic lipids, respectively. For the plots in Fig. 4 *B*, we used $A_{nl} = 70$ Å (Langmuir trough data), $r_{DOTAP} = r_{DMRIE} = 1$, $r_{DOSPA} = 2$, $Z_{DOTAP} = Z_{DMRIE} = 1$, and $Z_{DOSPA} = 3$. We found that values of Z_{DOSPA} between 3 and 4 yield a good visual fit for the comparison between DOTAP and DOSPA while 2 and 5 clearly do not. For environments of neutral pH we expect Z_{DOSPA} to be closer to 4. The value of Z_{DOSPA} could be regarded as a fitting parameter in the range between 3 and 4. Remarkably, given the complexity of the CL-DNA-cell system, the data, spread out when plotted as a function of Φ_{nl} (Fig. 4 *A*), coalesce into a ''universal'' curve as a function of σ_M, with TE varying exponentially over nearly four decades as σ_M increases by a factor of ≈ 8 (Fig. 4 *B*, σ_M between 0.0015 $e/\text{Å}^2$ and 0.012 $e/\text{Å}^2$), clearly demonstrating that σ_M is a key universal parameter for transfection with lamellar L_{α}^{C} CL-vectors. We now observe a single optimal $\sigma_M^* \approx 0.0104 \pm 0.0017\ e/\text{Å}^2 \approx e/(100\ \text{Å}^2)$ (Fig. 4 *B*, *arrow*) where the universal TE curve saturates for $\sigma_M > \sigma_M^*$ for both univalent and multivalent cationic lipid-containing CL-vectors. σ_M controls the average DNA interaxial spacing d_{DNA} (Fig. 2, *inset*), which decreases as σ_M increases (Koltover et al., 1999; Raedler et al., 1997). Future designs of CL-vectors, which further enhance the packing of DNA based on the recent theoretical understanding of intermolecular interactions within the complex (Bruinsma, 1998; Harries et al., 1998; O'Hern and Lubensky, 1998), may be expected to enhance TE.

The TE data suggest vastly diverse behaviors of L_{α}^{C} CL-DNA complexes between low and high σ_M. As we discussed earlier, for low $\sigma_M = e/(200\ \text{Å}^2)$ where TE is low, confocal images show DNA locked within complexes after endocytosis (Fig. 3 *B*). To test the idea that it is the endosomal vesicle that traps the complex, we carried out transfection experiments in the presence of chloroquine, a well-established bioassay known to enhance the release of trapped material within endosomes by osmotically bursting the vesicle. The endocytic pathway involves the fusion of endosomes with lysosomes (vesicles containing enzymes for degradation of material within endosomes) leading to late-stage endosomes, limiting the time available for CL-DNA complexes to escape. Chloroquine, a weak base, penetrates the lysosome and accumulates in a charged state; thus, lysosomes and late-stage endosomes tend to rupture due to increased osmotic pressure caused by counterions rushing in (Voet and Voet, 1995).

The fractional increase ($TE_{chloroquine}/TE$) for the DOSPA/DOPC and DOTAP/DOPC systems with added chloroquine as a function of σ_M (Fig. 4 *C*) shows the large increase in TE by as much as a factor of 60 as σ_M decreases and indicates that at low σ_M lamellar L_{α}^{C} complexes are trapped within endosomes, consistent both with the confocal images (Fig. 3 *B*) and the measured low TE without chloroquine. At high σ_M, chloroquine has a much smaller effect on TE with the frac-

DOCKET ALARM

Explore Litigation Insights

Docket Alarm provides insights to develop a more informed litigation strategy and the peace of mind of knowing you're on top of things.

Real-Time Litigation Alerts

Keep your litigation team up-to-date with **real-time alerts** and advanced team management tools built for the enterprise, all while greatly reducing PACER spend.

Our comprehensive service means we can handle Federal, State, and Administrative courts across the country.

Advanced Docket Research

With over 230 million records, Docket Alarm's cloud-native docket research platform finds what other services can't. Coverage includes Federal, State, plus PTAB, TTAB, ITC and NLRB decisions, all in one place.

Identify arguments that have been successful in the past with full text, pinpoint searching. Link to case law cited within any court document via Fastcase.

Analytics At Your Fingertips

Learn what happened the last time a particular judge, opposing counsel or company faced cases similar to yours.

Advanced out-of-the-box PTAB and TTAB analytics are always at your fingertips.

API

Docket Alarm offers a powerful API (application programming interface) to developers that want to integrate case filings into their apps.

LAW FIRMS
Build custom dashboards for your attorneys and clients with live data direct from the court.

Automate many repetitive legal tasks like conflict checks, document management, and marketing.

FINANCIAL INSTITUTIONS
Litigation and bankruptcy checks for companies and debtors.

E-DISCOVERY AND LEGAL VENDORS
Sync your system to PACER to automate legal marketing.